Refractive Indices of the Optically Nonlinear Organic Crystal (*S*)-3-Methyl-5-nitro-*N*-(1-phenylethyl)-2-pyridinamine

S. Lochran, R. T. Bailey, F. R. Cruickshank,* D. Pugh, J. N. Sherwood, and G. S. Simpson

Department Of Pure and Applied Chemistry, University Of Strathclyde, 295 Cathedral Street, Glasgow G1 1XL, U.K.

J. D. Wallis and P. J. Langley

Centre for Materials Research, School of Physical Sciences, The University of Kent, Canterbury, Kent CT2 7NH, U.K.

Received: March 31, 1998; In Final Form: May 27, 1998

The refractive indices of structurally well-characterized crystals of the new optically nonlinear organic crystal (*S*)-3-methyl-5-nitro-*N*-(1-phenylethyl)-2-pyridinamine have been measured from 480 to 660 nm and fitted to four-parameter Sellmeier equations with an accuracy of $\pm 3 \times 10^{-3}$ to $\pm 5 \times 10^{-3}$. The value of n_y was accurately verified by the measurement of the external angle of incidence required, at the (101) plane, to observe type I phase matching with a fundamental wavelength of 1064 nm. The phase matching locus has been established and is of Hobden class eight. The values of the n_x, n_y, and n_z refractive indices at 532 nm were found from the Sellmeier equations to be 1.690, 1.901, and 1.725, respectively, and their relative magnitudes are correlated with the molecular arrangement in the crystal lattice. This material is a member of a series of pyridinamines that can exhibit the phenomenon of frequency-dependent orientation of their dielectric axes. Since this compound crystallizes in an orthorhombic structure, rotation of the dielectric axes is precluded for symmetry reasons.

Introduction

Optical materials that possess large nonlinearities are of importance as frequency converters and modulators. Over the past few years, much interest has centered on conjugated organic molecules since they generally exhibit properties that surpass those of current inorganic materials.[1] From the initial discovery of the high-performance optically nonlinear material (*S*)-5-nitro-*N*-(1-phenylethyl)-2-pyridinamine (MBANP),[2] there has been an increase[3] in the work on benzylamine-substituted nitropyridine derivatives primarily owing to the large second-order polarizabilities of these molecules. The materials also show the property of frequency-dependent rotation of the dielectric axes about the crystallographic *b*-axis. This property can be exploited[2] to allow the use of the diagonal d_{ii} coefficients of $\chi^{(2)}$ in-phase matching, although this is normally forbidden. This is desirable, since these coefficients are often very large. (*S*)-3-Methyl-5-nitro-*N*-(1-phenylethyl)-2-pyridinamine (S3MeMBANP),[4] Figure 1, is a molecular organic compound that is a methyl-substituted derivative of (*S*)-5-nitro-*N*-(1-phenylethyl)-2-pyridinamine (MBANP) and has been previously identified as a promising, optically nonlinear material by the powder disk technique.[5,6] This powder efficiency can be interpreted only semiquantitatively, since only the transmitted radiation is detected. Despite this, the large, observed nonlinearity of S3MeMBANP justified single-crystal growth in order that a full optical characterization could be carried out. This lengthy process begins with an accurate determination of the linear optical properties of structurally well-characterized, crystalline materials as reported in the present work. This structural characterization is essential since the phase-matching efficiency has been shown to vary, for example, by a factor of 3 between samples cut from the highest quality and rather less high-quality growth sectors of the same crystal.[2]

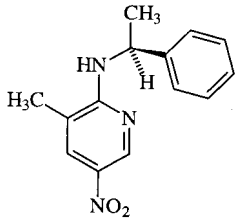

Figure 1. Structural formula of S3MeMBANP.

Crystal Growth and Topography

The success of the growth of high-quality single crystals is very much dependent on the purity of the starting material.[7] S3MeMBANP was purified by continuous-column chromatography,[8] which economically scales up the commonly practiced small-scale chromatography technique. Relatively large quantities, (10−100 g), of material were passed through the stationary phases used in the purification of S3MeMBANP. These were silica gel (mesh size 60−100) and alumina. The solvent used was dichloromethane. The apparatus used for such purification is shown schematically in Figure 2.

The starting material is placed in the flask fitted with a glass frit at the top of the column. The distilled solvent is placed in the flask at the bottom of the column and heated until boiling. The solvent vapor travels via the sidearm and condenses onto the material in the glass frit. The solution then passes through the frit and onto the stationary phase. The rate of condensation of vapor can be matched to the rate of solution flow through the PTFE tap at the base of the column so that the system remains equilibrated. Eventually all the material in the top flask is passed down through the stationary phase where the impurities are trapped, usually at the top of the column. S3MeMBANP was purified to 99.98% assayed by GLC using this method.

10.1021/jp981698u CCC: $15.00
Published on Web 07/31/1998

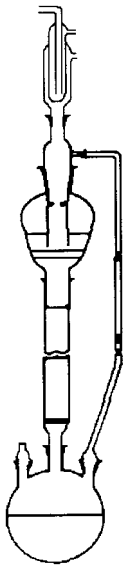

Figure 2. Continuous chromatography equipment.

Large single crystals of this material were grown by two methods. In the first method the crystal was grown from the melt by the Bridgman technique. Samples can be obtained in a matter of days by this method, but it results in crystals with no natural faces. Subsequent orientation using Laue camera techniques is possible, using a (001) cleavage plane as a reference plane. Dielectric planes of crystals grown by this method show complete extinction under a polarizing microscope.

The material may also be grown from solution in acetone by the temperature-lowering technique. This results in crystals with the habit shown in Figure 3. With optimized growth conditions, it has been possible to obtain large specimens (up to 40 × 40 × 15 mm^3). From crystal specimens obtained by both these methods, prisms have been cut and polished to optical tolerances allowing the accurate measurement of refractive indices.

The quality of the solution-grown crystals was evaluated by synchrotron, white light X-ray topography. The topograph, which essentially shows a projected cross-sectional view of the crystal, was obtained using a 50 μm high, collimated X-ray beam. The seed, which can be seen clearly at the right-hand side of Figure 4, is surrounded by a series of inclusions and refacetting defects normally associated with the initial stages of seeded solution growth. The uniform contrast of the remainder of the topograph defines its high quality. From the seed, surface dislocations propagate along the axis of the crystal. The specimens for optical characterization were cut from these high-quality regions, avoiding the dislocations, and hence are of very low, near zero, defect concentration.

The crystal structure of this material has been determined[4] to be orthorhombic, of space group $P2_12_12_1$ and point group 222. The lattice parameters are $a = 5.481(4)$ Å, $b = 6.791(8)$ Å, and $c = 35.88(3)$ Å at room temperature with four molecules per unit cell and a calculated density of 1.28 g cm^{-3}. It follows from the crystallographic symmetry that the dielectric axes coincide with the crystallographic axes and cannot rotate about the *b*-axis in this material, despite the fact that this molecule differs in structure from the monoclinic MBANP by only a methyl group.

Powder Tests

The powder technique used in the present work is a variation[5] of the original design of Kurtz and Perry[6] since the sample under study is prepared as a pressed potassium chloride disk. This

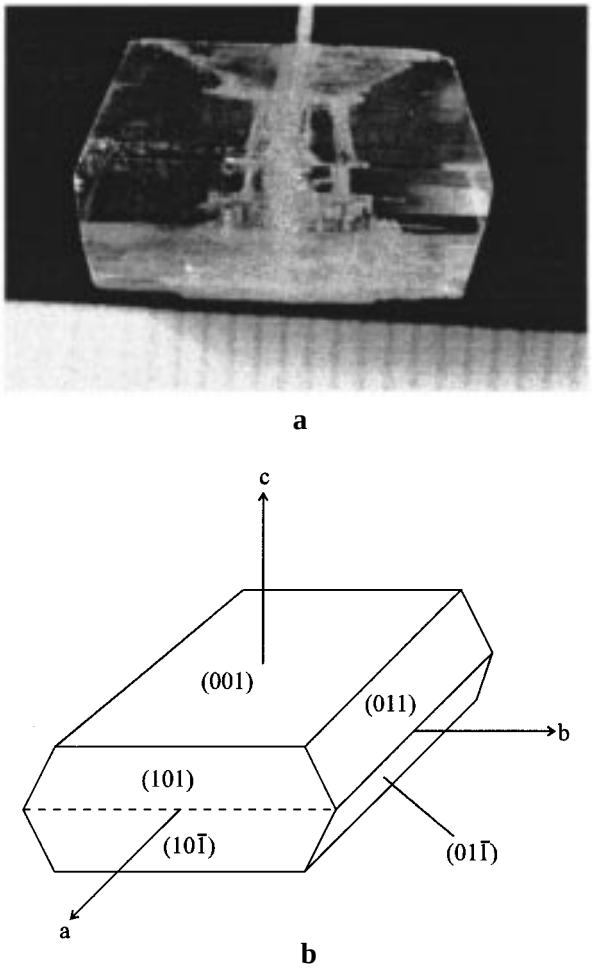

Figure 3. Morphology of (*S*)-3-methyl-5-nitro-*N*-(1-phenylethyl)-2-pyridinamine as obtained by the temperature lowering technique from a solution of acetone: (a) crystal grown from acetone; (b) crystal habit.

Figure 4. Thin section topograph of a solution-grown S3MeMBANP crystal with (010) as the input face. The seed is clearly seen on the right, and the growth dislocations arising from the seed are manifested by horizontal lines as the crystal grows.

alleviates the problem of trying to pack the nonlinear material, which, being an excellent insulator, readily charges electrostatically, making it difficult to produce a thin, uniform and compact layer.[9] The efficiency of the sample is determined by measuring the intensity of second harmonic radiation generated when a Nd:YAG laser is focused onto the disk. In addition, comparative measurements are made on a urea disk prepared in the same manner. A number of sites is examined in both cases. Laser power densities are kept well below 1 MW cm^{-2} to avoid the possibility of optically damaging the material.

Refractive Indices

To obtain a full understanding of the optically nonlinear behavior of materials, their refractive indices must first be accurately measured. The most common ways of achieving this are by using an Abbe refractometer,[10] the Becke line technique,[11] or the method of minimum deviation.[12] The first two techniques require that the material be in contact with a liquid of higher

refractive index. These methods are rarely suitable for molecular organic materials, since the existence of a liquid with such a refractive index and which is chemically inert toward the sample is unlikely. With the availability of large, high-quality, single crystals of S3MeMBANP, the minimum deviation method was chosen to evaluate the refractive indices, since this procedure yields values with an accuracy of typically ± 0.005 and is relatively insensitive to errors in the measurement of angles.

In order that all the principal refractive index dispersion curves could be measured, two prisms were prepared. The first prism was cut from a crystal obtained by the Bridgman technique. The axis of this prism was parallel to the crystallographic *c*-axis (*Z* dielectric axis), and the crystallographic *b*-axis (*Y* dielectric axis) was nearly parallel to the input face. The second prism was cut from the solution-grown crystal with its axis parallel to the crystallographic *a*-axis (*X* dielectric axis) and the crystallographic *b*-axis parallel to the input face. Both crystals were polished to a face flatness of better than $\lambda/5$ of sodium light using a Logitech PM-2 polishing machine, fitted with a Polytron-covered, cast-iron lapping plate. The polishing abrasive used was 0.3 μm alumina dispersed in paraffin oil.

The value of the principal refractive index, n_z, was determined, as a function of wavelength, in the first prism by the minimum deviation technique using a Hilger & Watts monochromator with a quartz-halogen light source.[13,14] The polarization, selected by a Glan-Thomson polarizer, was parallel to the prism axis. The value of the principal refractive index, n_x, was similarly determined in the second prism. In the first prism, the n_y refractive index was measured by using horizontally polarized light and plotting the effective refractive index as a function of angle of incidence calculated from the following equations

$$\theta_F = \theta_D - \theta_{inc} + \alpha$$

where θ_{inc} is the incidence angle to the prism, θ_F is the emergence angle from the prism, measured from the normal, θ_D is the deviation angle, and α is the prism apex angle. θ_F is calculated from measurements of θ_{inc}, θ_D, and α. The ratio $x = \sin \theta_{inc}/\sin \theta_F$ can then be evaluated followed by the refracted angle inside the prism, θ_R, calculated from

$$\tan \theta_R = (x \sin \alpha)/(1 + x \cos \alpha)$$

When this refracted angle is known, the effective refractive index, n_{eff}, can be calculated from Snell's Law

$$\sin \theta_{inc} = n_{eff} \sin \theta_R$$

The turning point in this plot is relatively insensitive to the angle of incidence and allows n_y to be determined more accurately than by solving pairs of simultaneous equations in n_x and n_y and n_z and n_y in the respective prisms.

Results and Discussion

The powder signal detected for S3MeMBANP was 17 times that of urea. This value indicates that this material possesses a large second-order optical nonlinearity and is well worth investigating in detail. Since its molecular structure is very similar to that of MBANP, analysis of the optical and structural differences between these two compounds should improve the understanding of the important features governing the symmetry of the lattice and the magnitude of the d_{ij} elements of $\chi^{(2)}$.

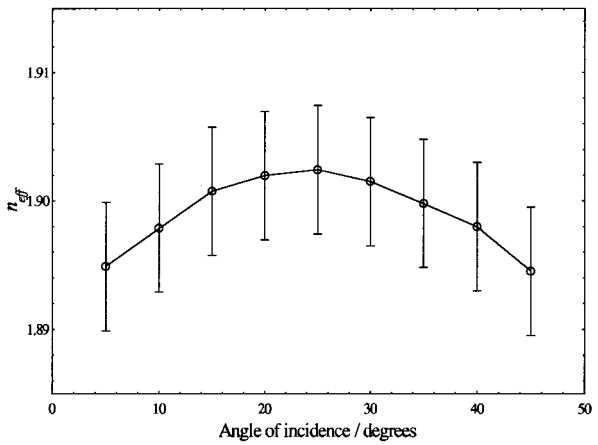

Figure 5. Plot of n_{eff} as a function of angle of incidence at 530 nm for a prism from the Bridgman grown crystal with the *Y* dielectric axis within the prism and perpendicular to the prism axis (*Z* dielectric axis) with the incident light horizontally polarized. The error bars represent an error of ± 0.005.

TABLE 1: Prism Apex Angles Used in Refractive Index Calculation

prism source	α/deg
Bridgman	16.700 ± 0.008
solution	13.467 ± 0.008

The apex angles of the two prisms prepared are shown in Table 1. The graph for n_y, using horizontally polarized light in the first prism, is shown in Figure 5 where the error bars represent ± 0.005. In the second prism the *Y* dielectric axis has been arranged to lie parallel to the input face, and hence the effective refractive index will pass through a maximum at normal incidence.

The values of the refractive indices measured were assessed to have an accuracy of ± 0.005 throughout the visible range. The refractive indices in the *Y* direction obtained from the two types of prism agreed with each other within the experimental error of ± 0.005. This reinforces the confidence in the measurements of n_y since the data were obtained independently and from different crystals and also verifies the accuracy with which the crystals were cut and polished in both cases. The accuracy of these measurements of refractive indices is due to the fact that very high optical quality faces can be obtained relatively easily with this material.

The values of n_x , n_y, and n_z were fitted to the four-parameter Sellmeier equation.

$$n_i^2 = A + \frac{B\lambda^2}{\lambda^2 - C} - D\lambda^2$$

where $i = x$, y, or z and λ is the wavelength in micrometers. Data were obtained at 5 nm intervals from 465 to 660 nm for n_x, at 10 nm intervals from 490 to 660 nm for n_y, and at 5 nm intervals from 470 to 660 nm for n_z. Data were also obtained at 1064 nm for n_y by adjusting its value until the observed incidence angle at which a type I phase matched signal was observed (31.5°) agreed with the calculated value. This allowed a refined Sellmeier fit for n_y as shown in Figure 6. A plot showing the remaining refractive indices together with the four-parameter Sellmeier fits and error bars is shown in Figure 7.

The values of the coefficients, with λ in micrometers, are shown in Table 2. These coefficients should be regarded as valid only in the wavelength range studied.

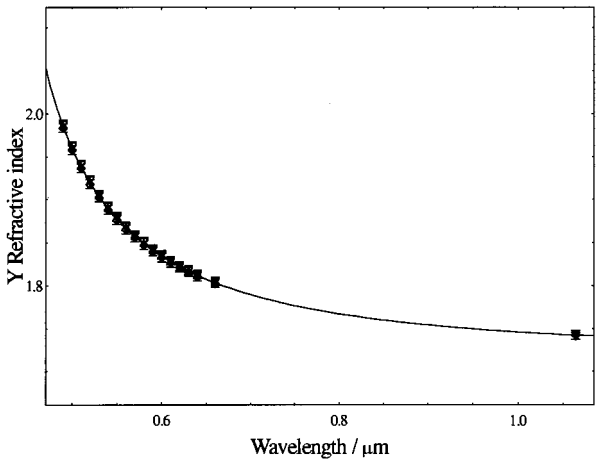

Figure 6. Plot of n_y with the fit to the Sellmeier equation and error bars.

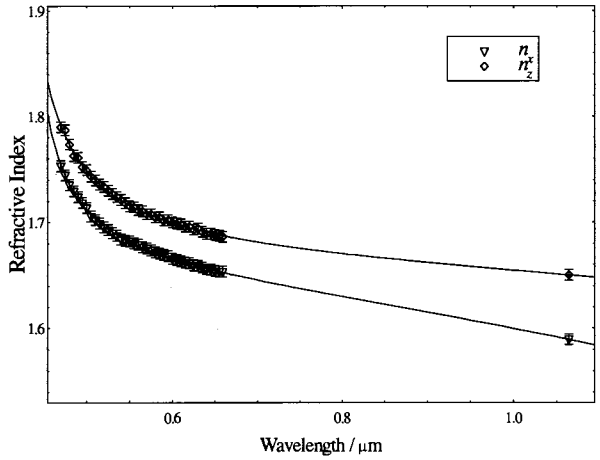

Figure 7. Data and four-parameter Sellmeier fit for n_x and n_z. Calculated data points at 1.064 μm are shown for comparison with Figure 6.

TABLE 2: Parameters Obtained for a Fit of the Refractive Index Data to the Four-Parameter Sellmeier Equation

	A	*B*	$C/\mu m^2$	$D/\mu m^{-2}$	max. dev.
n_x	2.780 36	0.063 708 9	0.184 186	0.374 153	2.53×10^{-3}
n_y	2.354 31	0.581 332	0.152 215	0.009 227 3	2.88×10^{-3}
n_z	2.635 22	0.153 796	0.163 522	0.081 165 3	5.1×10^{-3}

TABLE 3: Refractive Index Data Used To Construct the Phase-Matching Locus

	1064 nm	532 nm
n_x	1.5793	1.6896
n_y	1.7417	1.9014
n_z	1.6205	1.7254

The Sellmeier curves predict the refractive indices to within $\pm 2.5 \times 10^{-3}$ for n_x, $\pm 2.9 \times 10^{-3}$ for n_y, and $\pm 5.1 \times 10^{-3}$ for n_z. These curves lead to the values shown in Table 3 for refractive indices at a fundamental wavelength of 1064 nm and its second harmonic at 532 nm.

The order of the refractive indices used above places the phase matching in Hobden[13] class eight, and a stereographic projection of the phase-matching locus in the (001) plane is shown in Figure 8. Only type I phase matching is possible.

The relatively high values of n_y can be explained from the orientation of the molecules in the unit cell. The (100) projection is shown in Figure 9.

As can be seen from Figure 9 the charge-transfer axis is from the nitrogen atom of the amino group to the nitrogen atom of the nitro group. This results in this axis being the most polarizable axis of the crystal, and it makes an angle of 30.8° to the *Y* dielectric axis as calculated from X-ray data. It is therefore expected that the *Y* direction would, as observed, have the largest refractive index. This charge-transfer axis makes an angle of 66.1° with the *X*-axis and 71.8° with the *Z* dielectric axis. Although n_x has the lowest value, n_z is similar to it, being only 0.04 larger at 532 nm, for example.

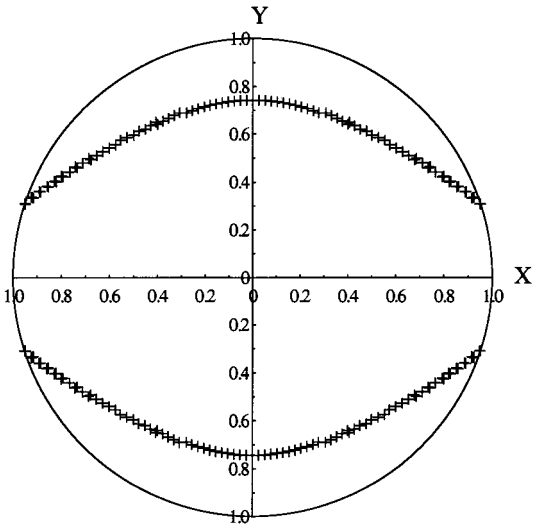

Figure 8. Stereographic projection of the phase-matching locus on the (001) plane for S3MeMBANP at a fundamental wavelength of 1064 nm. Only type I phase matching is possible in agreement with Hobden class 8.

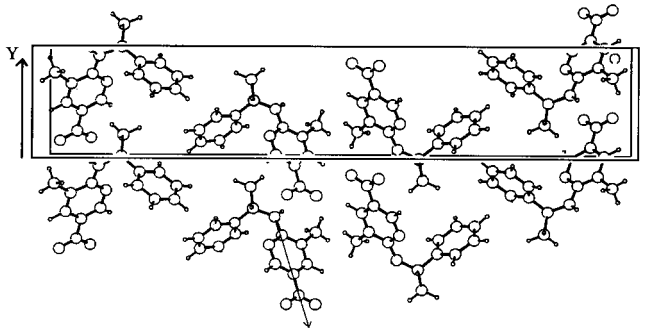

Figure 9. Orientation of S3MeMBANP molecules in the unit cell shown in the *bc*-plane. The arrow denotes the charge-transfer axis, which makes an angle of 30.8° with the *Y* dielectric axis.

In the solid state, absorption band centers for these materials cannot be determined in the visible spectrum because of their optical thickness, and so an estimated position is sought from solution spectra. The spectrum of a 5×10^{-5} M solution of S3MeMBANP in acetone was recorded, and the band center of the transition was found to be at 370 nm as shown in Figure 10.

The band center in cyclohexane was found to be 350 nm, showing only a small solvent shift. The transparency of S3MeMBANP in the solid state was determined using a Glan−Thomson polarizer in the sample arm of the instrument. Three optically polished samples of the bulk material with their input faces parallel to the (101), (110), and (001) crystallographic planes, respectively, were used in this characterization. The onset of the absorption edge, which is defined as the point at which the optical density has changed by 0.1, for light polarized in each direction is given in Table 4.

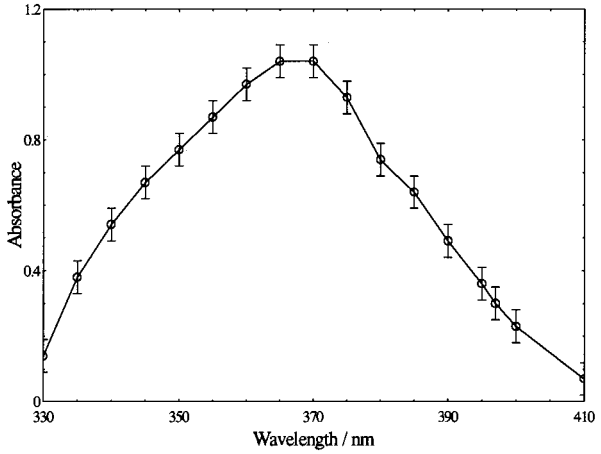

Figure 10. Solution spectrum of S3MeMBANP in acetone where *A* is in absorbance units. The band center occurs at 370 nm.

TABLE 4: Positions of Absorption Edges and Band Center Predictions

direction	edge/nm	$\sqrt{C}$/nm
X	465	429
Y	500	390
Z	480	404

The value of the absorbance at 600 nm was subtracted from all subsequent measurements to determine the change in optical density.

The specific rotation of S3MeMBANP was measured in solution in dichloromethane and was $[\alpha]_D^{25} = 191°$ dm^{-1} cm^3 g^{-1}, which is similar to that of MBANP for which $[\alpha]_D^{25} = 239°$ dm^{-1} cm^3 g^{-1}.

From Table 3, the refractive indices of S3MeMBANP are seen to be in the order $n_y > n_z > n_x$, and from Table 4 the onset of absorption for light, polarized in the *Y* direction, is seen to occur at the longest wavelength and at the shortest wavelength for light polarized in the *X* direction. This is consistent with the simple model that predicts that the direction of largest refractive index possesses an absorption edge at the longest wavelength. This model assumes that the refractive indices for each direction are essentially equal at very long wavelengths. Therefore, as the wavelength is decreased, it can be seen that the direction with the largest refractive index will approach a transition before the directions with smaller refractive indices and hence the absorption edge will appear at longer wavelengths for this direction.

The Sellmeier function is a four-parameter fit, and the parameters obtained from such a fitting process are highly dependent on the starting points given. Therefore, the prediction of the positions of the band centers using the square root of the Sellmeier *C* parameter do not hold any serious validity. Even the order of band centers predicted by the $\sqrt{C}$ values is incorrect as shown in Table 4. This agrees with our previous experience.

Conclusions

The three principal refractive indices of S3MeMBANP, an MBANP analogue, have been measured between 470 and 660 nm and fitted to four-parameter Sellmeier curves. A data point at 1064 nm was obtained by the fitting of theoretical phase-matching incidence angles to experimentally determined angles. From this, refined Sellmeier parameters for n_y were obtained, although the differences from the extrapolation of the visible wavelength data were scarcely significant. In this material the n_y refractive index was found to be the largest, which correlates

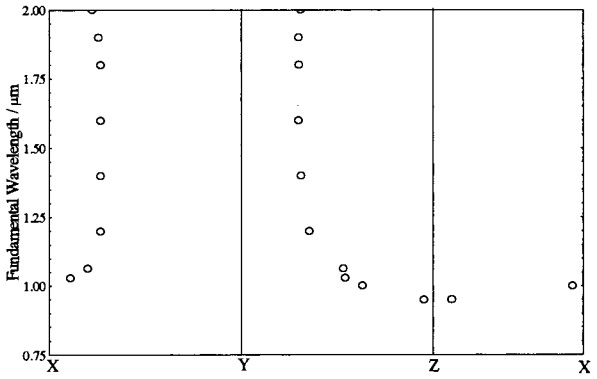

Figure 11. Phase-matching criticality curves.

with the charge-transfer axis making an angle of 30.8° with the *Y* dielectric axis. The values of n_x and n_z are similar, differing typically by 0.04, n_z being the larger. This is to be expected, given that the *X* and *Z* dielectric axes make similar angles with the charge-transfer axis. This correlation between refractive index and alignment with molecular charge-transfer axes has now been observed in several cases. In MBANP itself[2], the molecular charge-transfer axis makes an angle of 33.3° with the *Y* dielectric axis, resulting in n_y being the largest refractive index, the angles made with the other dielectric axes being larger. More recently, the correlation has been observed in the MBANP racemate[3] with the refractive indices following the exact order of the magnitudes of the projections of the molecular charge-transfer axis on the dielectric axes. The generality of these correlations provides strong evidence for the polarizability behavior of these compounds being that of an oriented gas model where the molecules are not significantly influenced by their neighbors in the lattice.

The orthorhombic symmetry of the crystal precludes the possibility of frequency-dependent orientation of the dielectric axes in this material. Clearly, the subtleties of the intermolecular forces have caused this packing rather than the monoclinic systems of MBANP and its racemate, although the two molecules differ only by the presence of the methyl group on the pyridine ring.

Thus the possibility of rotation of the dielectric axes depends on these two relatively independent effects, i.e., intermolecular forces as well as on the polarizability of the material in the $X-Z$ plane, which is relatively insensitive to these forces. In a uniaxial crystal, the dielectric axes are free to rotate about the *Y* dielectric axis, and it may be expected that a low birefringence in the $X-Z$ plane would lead to the frequency-dependent rotation of these axes in a monoclinic (biaxial) system. In the case of S3MeMBANP, the n_x and n_z values are within 0.04 typically, which is a smaller difference than is found in MBANP where the axes do rotate. It may therefore be concluded that, although this material exhibits very low dispersion in the $x-z$ plane, the intermolecular forces are the controlling feature preventing frequency-dependent rotation of the dielectric axes by the symmetry of the lattice packing arrangement.

The two prisms in this work were cut from crystals grown by two different methods. Although the Bridgman method frequently produces crystals with larger concentrations of dislocations and defects than solution growth, the close correspondence of the n_y refractive indices in the two prisms, cut from the highest quality volumes of each, suggests that the crystals were of similarly high optical quality.

The phase-matching locus of S3MeMBANP was calculated at a variety of fundamental wavelengths, using the Sellmeier

data above. A plot of wavelength versus the position in which the phase-matched locus intersects a principal dielectric plane is known as a criticality curve. From the criticality curve of S3MeMBANP shown in Figure 11 it is clear that this material is angle noncritical at wavelengths close to 950 nm (where there is little change in the wavelength with angle) and is wavelength noncritical at wavelengths from 1.25 to 2.00 μm (where there is little change in angle, and therefore phase-matched tuning geometry, as the wavelength changes).

Acknowledgment. The authors thank E. E. A. Shepherd for crystal purification and growth and the Engineering and Physical Science Research Council (EPSRC) for the financial support of this work.

References and Notes

(1) Garito, A. F.; Singer, K. D. *Laser Focus Fiberopt. Technol.* **1982,** *18*, 59.

(2) (a) Twieg, R. J.; Jain, K.; Cheng, Y. Y.; Crowley, J. S.; Azema, A. *Polym. Rep.* **1982**, *23*, 147. (b) Nayar, B. K.; Kashyap, R.; White, K. I.; Bailey, R. T.; Cruickshank, F. R.; Guthrie, S. M. G.; McArdle, B. J.; Morrison, H.; Pugh, D.; Shepherd, E. A.; Sherwood, J. N.; Yoon, C. S. *J. Mod. Opt.* **1988**, *35*, 511. (c) Bailey, R. T.; Cruickshank, F. R.; Guthrie, S. M. G.; McArdle, B. J.; Morrison, H.; Pugh, D.; Shepherd, E. A.; Sherwood, J. N.; Yoon, C. S. *Optics Commun.* **1988**, *65*, 229. (d) Bailey, R. T.; Cruickshank, F. R.; Kerkoc, P.; Pugh, D.; Sherwood, J. N. *J. Appl. Phys.* **1993**, *74*, 3047. (e) Bailey, R. T.; Cruickshank, F. R.; Pugh, D.; Sherwood, J. N. *J. Phys. D: Appl. Phys.* **1993**, *26*, 208. (f) Bailey, R. T.; Bourhill, G. H.; Cruickshank, F. R.; Pugh, D.; Simpson, G. S.; Sherwood, J. N. *J. Appl. Phys*, **1993**, *73*, 1591. (g) Bailey, R. T.; Cruickshank, F. R.; Kerkoc, P.; Pugh, D.; Sherwood, J. N. *J. Appl. Phys.* **1995**, *79*, 602.

(3) Kondo, T.; Akase, F.; Kumagai, M.; Ito, R. *Opt. Rev.* **1995**, *2*, 128.

(4) Twieg, R.; Azema, A.; Jain, K.; Cheng, Y. Y. *Chem. Phys. Lett.* **1982**, *92*, 208.

(5) Bailey, R. T.; Blaney, S.; Cruickshank, F. R.; Guthrie, S. M. G.; Pugh, D.; Sherwood, J. N. *Appl. Phys.* **1988,** *B 47*, 83.

(6) Kurtz, S. K.; Perry, J. *J. Appl. Phys.* **1968**, *39*, 3798.

(7) Bailey, R. T.; Cruickshank, F. R.; Pugh, D.; Sherwood, J. N. *J. Optoelectron.* **1990**, *5*, 89.

(8) Sangster, R. C.; Irvine, J. W. *J. Chem. Phys.* **1954**, *54*, 670.

(9) Bailey, R. T.; Cruickshank, F. R.; Pugh, D.; Sherwood, J. N. *Acta Crystallogr.* **1991**, *A 47*, 145.

(10) Tilton, L. W. *J. Opt. Soc. Am.* **1942**, *32*, 371.

(11) *Practical Optical Crystallography*; Hartshorne, N. H., Stuart, A., Eds.; Arnold: London; 1964, p 159.

(12) Tentori, D.; Lerma, J. R. *Opt. Eng.* **1990**, *29*, 160.

(13) Bailey, R. T.; Cruickshank, F. R.; Pugh, D.; Sherwood, J. N.; Simpson, G. S.; Wilkie, S. *J. Appl. Phys.* **1995**, *78*, 2, 1388.

(14) Bailey, R. T.; Cruickshank, F. R.; Pugh, D.; Sherwood, J. N. *J. Phys. D: Appl. Phys.* **1993**, *26*, B208.

(15) Hobden, M. V. *J. Appl. Phys.* **1967**, *38*, 4365.